Superconductor Science and Technology

PAPER • OPEN ACCESS

Soft-magnetic coatings as possible sensors for magnetic imaging of superconductors

OPEN ACCESS
IOP Publishing
Superconductor Science and Technology
Supercond. Sci. Technol. **33** (2020) 015002 (7pp)
https://doi.org/10.1088/1361-6668/ab5984

Soft-magnetic coatings as possible sensors for magnetic imaging of superconductors

A M Ionescu[1,2,5], J Simmendinger[1], M Bihler[1], C Miksch[1], P Fischer[1], S Soltan[3,1], G Schütz[1] and J Albrecht[4]

[1] Max Planck Institute for Intelligent Systems, Heisenbergstr. 3, D-70569 Stuttgart, Germany
[2] National Institute of Materials Physics, Atomistilor 405A, 077125, Magurele, Romania
[3] Department of Physics, Faculty of Science, Helwan University, Cairo 11792, Egypt
[4] Research Institute for Innovative Surfaces FINO, Aalen University, Beethovenstr. 1, D-73430 Aalen, Germany

E-mail: ionescu@is.mpg.de

Received 21 August 2019, revised 10 October 2019
Accepted for publication 20 November 2019
Published 6 December 2019

Abstract

Magnetic imaging of superconductors typically requires a soft-magnetic material placed on top of the superconductor to probe local magnetic fields. For reasonable results the influence of the magnet onto the superconductor has to be small. Thin YBCO films with soft-magnetic coatings are investigated using SQUID magnetometry. Detailed measurements of the magnetic moment as a function of temperature, magnetic field and time have been performed for different heterostructures. It is found that the modification of the superconducting transport in these heterostructures strongly depends on the magnetic and structural properties of the soft-magnetic material. This effect is especially pronounced for an inhomogeneous coating consisting of ferromagnetic nanoparticles.

Keywords: magnetic imaging, superconductor-ferromagnet heterostructures, critical current density, pinning in superconductors

(Some figures may appear in colour only in the online journal)

Introduction

Owing to its unique properties $YBa_2Cu_3O_{7-x}$ (YBCO) is one of the most promising superconductors for large-scale applications such as superconducting power cables, motors, magnetic energy-storage devices, fault current limiters and transformers [1, 2]. The development of superconducting applications is closely related to a successful characterization of the electric transport in the material. A promising characterization method is the spatially resolved analysis by magnetic imaging such as magneto-optical imaging [3–6] or x-ray microscopy [7, 8]. Magnetic scanning transmission x-ray microscopy utilizes dichroic absorption and thus, unlike other methods, does not have to distinguish between either resolution, small magnetic fields, surface roughness, polarity sensitivity or tip coercivity. An important point here is that magnetic field distributions can be visualized with high spatial resolution at low temperatures [8]. For this purpose a ferromagnetic material has to be brought in close contact with the superconductor. This typically leads to a variety of coupling phenomena such as proximity [9–12] and inverse proximity effects [13, 14], spin–orbit coupling [15, 16] or dipolar coupling [17, 18].

For a feasible sensor layer one of the most important requirements is that it has to probe local magnetic fields of the superconductor without changing its properties. Thus, to avoid proximity effects [19] a thin insulating layer is introduced at the SC/FM interface [20], whereby the SC/FM interaction is governed by dipolar coupling [17, 18]. As of today, numerous ferromagnetic materials have been used as sensor layers for magnetic imaging, such as thin films of amorphous $Co_{40}Fe_{40}B_{20}$ [21–23] $Fe_{20}Ni_{80}$ (permalloy, Py) [8, 17] or epitaxial $La_{2/3}Ca_{1/3}MnO_3$ (LCMO) [24].

[5] Author to whom any correspondence should be addressed.

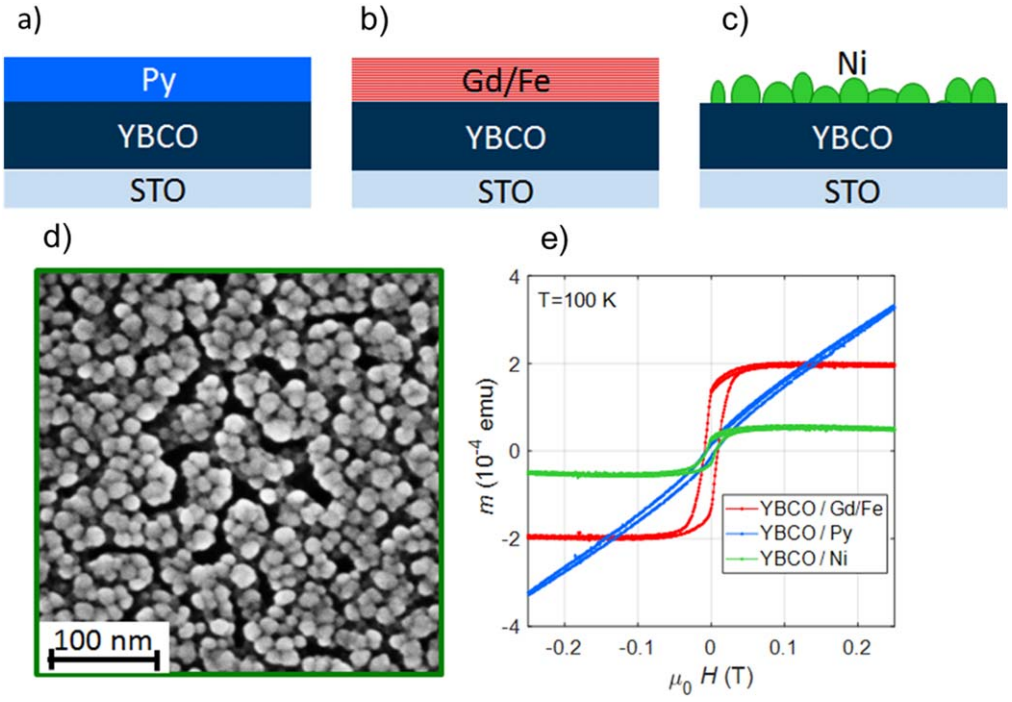

Figure 1. Schematics of the SC/FM bilayers consisting of YBCO and (a) Py, (b) Gd/Fe and (c) Ni-nanoparticles. (d) SEM micrograph of the Ni nanoparticles on top of YBCO (e) magnetic hysteresis curves of the SC/FM bilayers measured at 100 K.

In a typical imaging experiment the superconducting material is cooled in the absence of a magnetic field. Afterwards an external magnetic field is applied that leads to the penetration of magnetic flux into the superconductor. The penetration is governed by pinning of magnetic vortices. The efficiency of pinning is proportional to the magnitude of the critical current density. Since the London penetration depth λ in YBCO is much larger than the coherence length ξ, vortex core pinning is usually the dominant mechanism at low temperatures [25]. Several methods to create natural and artificial pinning centers have been developed such as the creation of oxygen vacancies [26], microstructural variations [27, 28] or the addition of secondary phases [29, 30]. A main prerequisite of a sensor layer is that it does not provide additional pinning caused by its magnetic structure.

In this work, we investigate bilayers consisting of a YBCO thin film and a (soft-) ferromagnetic layer. We explore how the interaction between the superconductor and the ferromagnet leads to a change in superconducting transport. Only if these changes are reasonably small is the material an efficient sensor layer. Further insight is gained from the temperature dependence of the critical current density and relaxation measurements.

Sample preparation

We used pulsed-laser deposition to epitaxially grow 200 nm thick films of optimally doped YBCO on single-crystalline $SrTiO_3$ (001) substrates with a lateral size of $5 \times 5\,mm^2$.

On three identical YBCO films, ferromagnetic layers were deposited: 50 nm of Permalloy (Py) with magnetic in-plane anisotropy, 35 nm of Fe/Gd multilayers consisting of 25 layers of each Fe and Gd with individual thicknesses of 0.7 nm having out-of-plane anisotropy and randomly ordered Ni nanoparticles with diameters of 10–20 nm. The ferromagnetic materials have been chosen to study the influence of different magnetic and morphological properties of the sensor layers on the transport in the superconductor.

Py and Gd/Fe layers were deposited using ion beam sputtering in UHV atmosphere at room temperature. A 5 nm STO buffer layer was introduced at the SC/FM interface for all bilayers. Physical vapor deposition with glancing angle deposition (GLAD) was used to coat the superconductor surface with Ni nanoparticles. A glancing angle of 83° and fast rotation of the substrate around its azimuthal axis were applied during the Ni deposition to obtain the magnetic nanoparticles shown in the SEM image in figure 1(d). Details of the GLAD set up can be found in [31].

A sketch of the samples is depicted in figures 1(a)–(c). The SEM image in figure 1(d) shows the surface of the Ni nanoparticle distribution on top of the YBCO surface. Herein, individual Ni particles with typical diameters of 10–20 nm form larger agglomerates.

All samples were characterized by SQUID magnetometry using a Quantum Design MPMS3. The external magnetic field $\mu_0 H$ was applied perpendicular to the plane of the sample. The critical temperature T_c was measured in an applied field of 1 mT, after the samples were cooled in zero field. The T_c for the reference sample is 88 K, in case of Py and GdFe we find $T_c = 88.4$ K and in case of Ni $T_c = 92$ K. The slight variations of T_c do not affect the conclusions of this work.

Figure 1(e) shows the hysteresis curves measured with a sweeping rate of 5 Oe s^{-1} at 100 K above the superconducting

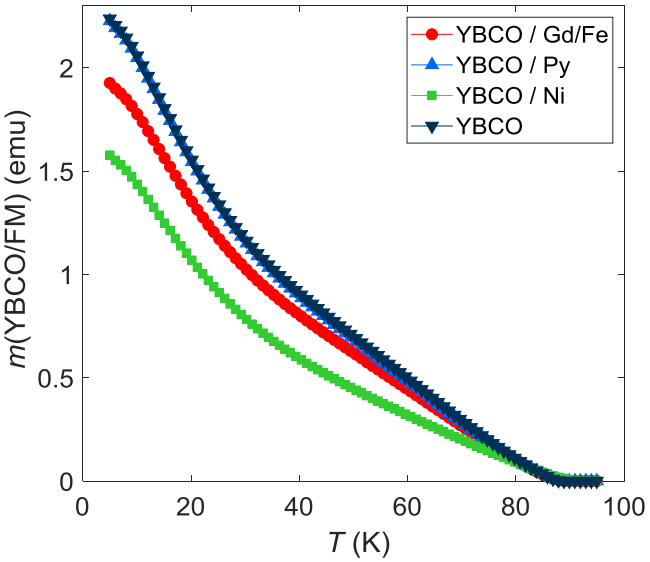

Figure 2. Temperature-dependent magnetic moment $m(T)$ in the remanent state of reference sample (black), Py (blue), Fe/Gd (red) and Ni (green).

transition. The Py (blue) and the Gd/Fe (red) sample show the expected behavior of a thin film with in-plane and out-of-plane anisotropy, respectively. Ni nanoparticles (green) behave like an isotropic magnet due to the approximately round shape of the individual particles. All ferromagnetic layers exhibit a similar coercive field of $\mu_0 H_c \sim 10$ mT, but different magnetic moments at saturation: 8.5×10^{-4} emu for Py; 2×10^{-4} emu for Gd/Fe and 0.5×10^{-4} emu for the layer with Ni nanoparticles.

The magnetic moment m is measured below T_c to reveal the influence of the different magnetic layers on the transport in the superconductor. Figure 2 depicts the temperature-dependent magnetic moment of the single YBCO layer (reference sample) and the YBCO/FM bilayers. The magnetic moment has been measured in the remanent state after cooling the sample through its superconducting transition in zero field to a temperature $T = 5$ K and applying out-of-plane an external magnetic field $\mu_0 H_{ex} = 0.3$ T for several seconds. Subsequently, the external field is reduced to zero and the magnetic moment is measured while continuously heating the sample to 100 K.

It can be seen that all samples behave in a similar way: a large magnetic moment at low temperatures monotonically decreases while heating up towards T_c. The deposition of the ferromagnetic layers leads to a suppression of the magnetic moment. In case of Py (blue) this suppression is vanishingly small even though Py has the highest magnetic moment at saturation, it increases for Fe/Gd (red) (intermediate m at saturation) and is considerable increased for Ni nanoparticles (green). We find that neither the saturation magnetization nor the coercivity are important for the dipolar coupling to the superconductor. The morphology of the magnetic stray field changes significantly from the homogeneous Py layer via the Fe/Gd multilayer to the nanoparticle agglomerate. This seems to be important for the description of the influence of the ferromagnet to the superconductor.

In [21], the suppression of the magnetic moment is ascribed to mechanical damage during the deposition process. We assume that the interaction of the superconductor with the ferromagnet is limited to magnetic coupling through introduction of the 5 nm STO decoupling layer. In this case, only the stray field configuration can have impact on the transport in YBCO.

In figure 3(a) we plot the ratio r of the critical current density before and after the coating of identical YBCO films with different ferromagnetic layers. To extract the critical current density, J_c, the Bean relation has been applied [32] modified for a plate-like geometry [33]:

$$J_c(\mathrm{A\,cm^{-2}}) = 60|m(emu)|/V(\mathrm{cm^3}) \cdot l(\mathrm{cm}),$$

where, V the sample volume , and l the basal square side.

In the range of 5–80 K the ratio r is constant for the Py sample and close to unity (blue). The Gd/Fe sample shows slightly smaller values of $r = 0.95$ (red). In case of Ni nanoparticles a severe suppression of about 25% is found (green). In this representation it is also seen that at temperatures close to T_c (>80 K) an increase of J_c is found compared to the reference sample. This increase is smallest in case of the Py film, intermediate for the Fe/Gd multilayer and largest for Ni nanoparticles.

The introduction of the decoupling layer weakens the influence of the ferromagnet on the superconducting state at the interface. The origin of the increase of J_c at high temperatures is magnetic pinning of the superconducting vortices by the inhomogeneous magnetization of the ferromagnet [34, 35]. Thus, the effect increases from Py via Fe/Gd to Ni nanoparticles.

The increase of m close to T_c can nicely be seen when performing a $m(H)$ measurement. The result for the Ni nanoparticle decoration is depicted in figure 3(b) where the hysteresis loops have been measured at $T = 85$ K. Similar results have been found for CoFeB [20, 21]. Pinning is affected much stronger in the presence of the inhomogeneous arrangement of Ni nanoparticles compared to the anisotropic but homogeneous Py and Fe/Gd films.

The temperature dependence of the critical current density can give detailed insight into the pinning mechanisms [27, 28, 36]. The critical current density J_c can be described by a power law

$$J_c(T) = J_c(0)(1 - T/T_c)^s, \quad (1)$$

where the exponent s contains information about the pinning mechanism in the superconductor. This scaling behavior can be applied for pinning when there is no applied field and where collective processes can be neglected [37, 38]. Note, that the 'zero field condition' can not be fully fulfilled in macroscopic films. The self-field of the supercurrents leads to vortex interactions and to a smearing out of the power-law behavior [38]. For many superconductors $J_c(T)$ can be fitted over the whole temperature range with a fixed exponent $s = 1.5$ [39].

In case of YBCO thin films normally two separated temperature regimes with different exponents arise. At around $T \sim 40$ K a crossover of the exponent $s$is found, indicating a modification of the fundamental pinning mechanism [38].

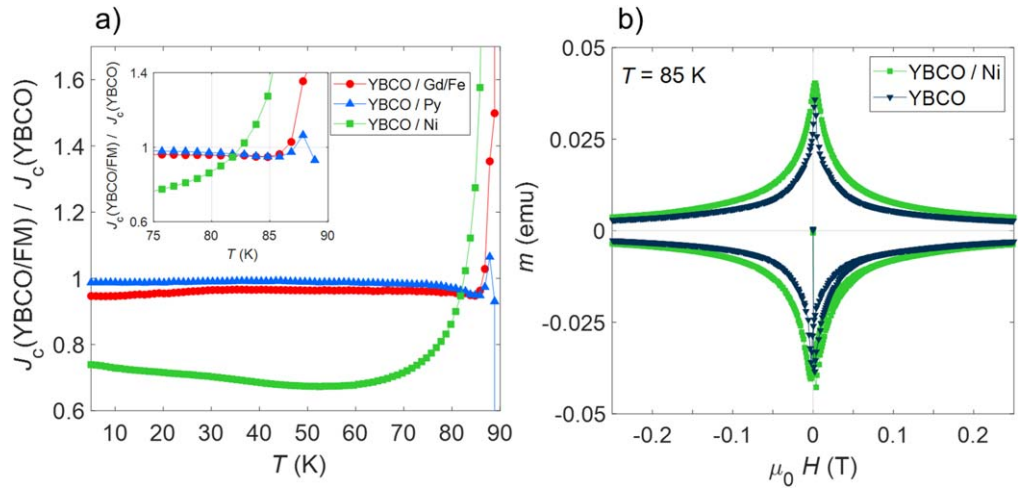

Figure 3. (a) Ratio r of the critical current densities J_c(YBCO/FM) and J_c(YBCO) as a function of temperature T. The ratio is close to unity independent of temperature for the Gd/Fe (red) and Py (blue) samples and it takes smaller values for the Ni (green) in the 5–80 K range. (b) Hysteresis loops of the reference sample and the Ni sample measured at 85 K.

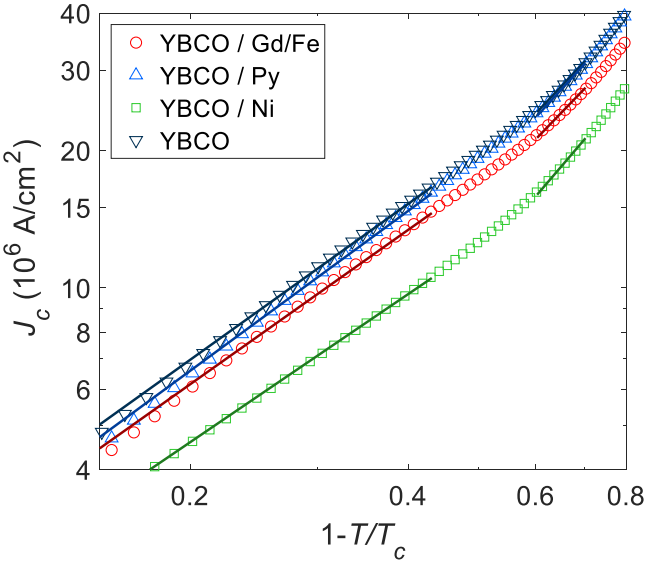

Figure 4. Temperature dependence of the critical current density for the YBCO single layer and the three bilayers with Gd/Fe, Py or Ni. Continuous lines represent the power law $J_c = (1-T/T_c)^s$ fit to obtain s.

Table 1. The exponent s for all samples in the low and high temperature range, errors are below 0.05.

Sample/s	s(20–35 K)	s(50–80 K)
YBCO	1.68	1.14
YBCO/GdFe	1.64	1.12
YBCO/Py	1.73	1.16
YBCO/Ni	1.85	1.08

Above 40 K, s is about unity, which can be explained by thermally activated depinning of flux lines. Below 40 K, the dominant mechanism is vortex core pinning, the corresponding exponent s is 1.5 [38]. For YBCO thin films with a grain boundary free current, the value 1.5 was found experimentally [40] and theoretically [37, 38, 40].

The change of s, which can be observed in figure 4 emphasizes the existence of two temperature regimes with different vortex-depinning mechanisms. The values of s are represented in table 1 and the errors are below 0.05. For temperatures above $T = 50$ K where $s \sim 1.1$ for almost all samples, the continuous ferromagnetic layers produce no change in $J_c(T)$ and the thermally activated depinning is the dominant pinning mechanism. The isotropic properties of Ni nanoparticles have a significant impact on the pinning properties, as is indicated by a higher s. Below 35 K we identified exponents higher than $s \sim 1.5$ [40]. For the reference sample, we find $s = 1.68$. This is a clear footprint for additional inhomogeneities which are known to increase s [38]. The exponents found for the Py and Gd/Fe samples are similar to the one for the reference sample, meaning that the influence of these ferromagnetic layers is not important on the J_c. In contrast, the largest exponent s obtained for Ni indicates that the stronger decay of the currents with temperature is due to a magnetically induced inhomogeneity [41]. It is shown that the morphology of the ferromagnetic layers (homogeneous film for Py, multilayered structure for Gd/Fe and nanoparticles for Ni) and the orientation of the easy axis have an important contribution to the behavior of the superconductor.

Since thermally activated depinning plays an important role in vortex movement, we analyze the corresponding pinning energies by a relaxation experiment: the sample is zero field cooled to different temperatures, a magnetic field of 0.2 T is applied and the decay of the magnetic moment in time $m(t)$ is recorded for a time window t_w of 45 min. In the range where $\ln(|m|)$ versus $\ln(t)$ is linear, i.e. not too close to the irreversibility line and for a moderate relaxation time window t_w, we can extract the normalized vortex-creep activation energy

$$U^* = -T\Delta\ln(t)/\Delta\ln(|m|) \quad (2)$$

averaged over t_w [42]. U^* increases with temperature in the collective (elastic) vortex-creep regime (ordered vortex phase)

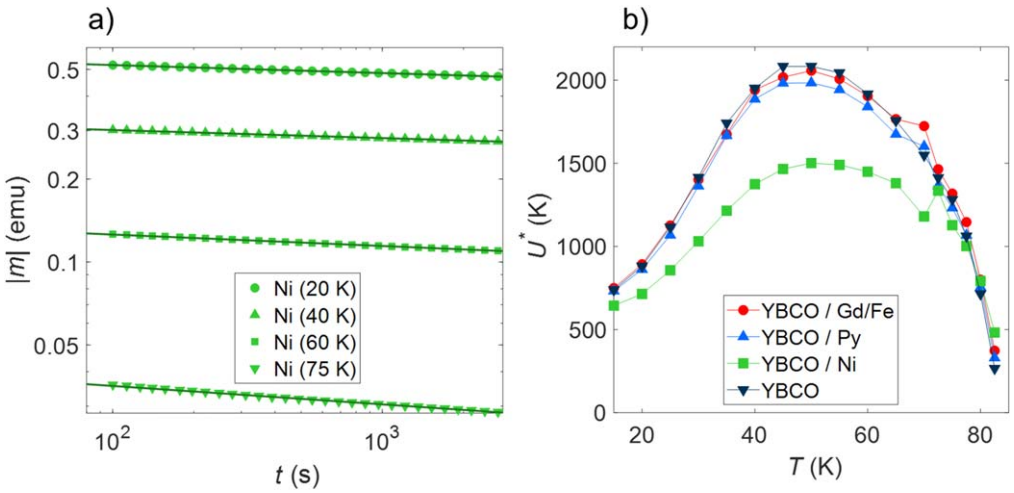

Figure 5. (a) Magnetic relaxation curves |m| versus t at several temperatures for YBCO/Ni sample (in $\mu_0 H = 0.2$ T), from which the normalized vortex-creep activation energy U^* was extracted. The continuous lines represent a linear fit. b) The resulting U^* increases with increasing temperature in the low-T range, exhibiting a maximum at ~50 K, where $U^* = U_c$ (the characteristic pinning energy).

[43] and decreases for plastic (dislocation mediated) creep (disordered vortex phase) [44].

Figure 5(a) illustrates several magnetic relaxation curves (in a log–log plot) measured for the Ni decorated YBCO film at different temperatures. All resulting curves exhibit a typical linear behavior (figure 5(a)), therefore U^* can be extracted using equation (2) [34]. Compared to the reference sample, the Py and Gd/Fe samples behave nearly identical, as seen in figure 5(b). In contrast, the addition of Ni nanoparticles leads to a decrease of the maximum value of U^* of about 25%, again showing that Ni has the largest influence on the superconducting transport properties. In case of Py and Fe/Gd the influence on the magnetic relaxation is small. Py exhibits a slightly larger effect than Fe/Gd showing that relaxation experiments illuminate different properties of the superconducting transport.

For all samples U^* increases with temperature in the interval 5–50 K indicating an ordered vortex phase, at higher temperatures U^* decreases, due to plastic creep. At the crossover temperature, U^* can be identified with the characteristic pinning energy U_c. The $U^*(T)$ dependence has been intensively studied for YBCO films with different pinning centers [45]. It has been observed that the crossover collective creep—plastic creep always appears in DC magnetization relaxation measurements in samples with random pinning. The crossover can be understood in terms of an energy balance relation, where the thermal energy can be neglected for strongly pinned samples and T significantly below T_c. At low T, the relaxation is smaller leading to a J closer to J_c, the effective pinning is weak and the intervortex interactions play an important role, giving rise to collective pinning. At high T the energy balance changes, because J relaxes faster and U increases. In these conditions, in the vortex system appear dislocations due to vortex pinning and the creep becomes plastic. Roughly, this dynamic crossover appears when the effective depth of the pinning potential well equals the vortex deformation energy [25].

The SC/FM interaction was intensively studied as for example in [21] where a suppression of the magnetic moment was also observed. In that work, the main factor that lead to suppression was the deposition process, which affected the superconductor at the surface and many coupling phenomena were present. At high temperatures, magnetic pinning comes into play, and the J_c is increased compared to the pristine YBCO film. For our study, the introduction of the STO decoupling restricts the SC/FM to magnetic coupling through the stray fields arising from the ferromagnet. The homogeneous in-plane easy axis film of Py provides almost no stray fields, except at the edges, the multilayered structure for Gd/Fe (out of plane easy axis) determines more intense stray fields and the Ni nanoparticles (isotropic) have the highest stray fields which penetrate into the superconductor. The magnitude of the stray field is proportional with the suppression of J_c. Over 80 K magnetic pinning becomes efficient.

Conclusion

In summary, we investigated the influence of various (soft)-ferromagnetic coatings on the current transport in high temperature superconducting YBCO thin films. Ferromagnets showing a negligible influence on the critical current density of the superconductor can be used as efficient sensor materials for magnetic imaging at low temperatures. We analyze heterostructures of YBCO thin films and ferromagnetic coatings of either Py layers, Gd/Fe multilayers or Ni nanoparticles. We find that the influence on the superconducting properties increases from in-plane to perpendicular easy axis of the ferromagnet. In addition, an inhomogeneous microstructure leads to the largest effects. This means that the homogeneity and anisotropy of the magnetic structure are decisive for the superconducting transport. Both the coercivity and the saturation magnetization of the ferromagnet do not play substantial roles. Finally, we have identified a thin Py layer as

an ideal candidate for magnetic imaging in particular in the x-ray regime.

The authors are grateful to G Cristiani and B. Ludescher (MPI Stuttgart) for their contributions to the sample fabrication.

ORCID iDs

A M Ionescu https://orcid.org/0000-0001-7357-4249
J Albrecht https://orcid.org/0000-0002-4047-4302

References

[1] Foltyn S R, Civale L, Jia Q X, Maiorov B, Wang H and Maley M 2007 Materials science challenges for high-temperature superconducting wire *Nat. Mater.* **6** 631–42
[2] Larbalestier D, Gurevich A, Feldmann D M and Polyanskii A 2001 High-Tc superconducting materials for electric power applications *Nature* **414** 368–77
[3] Jooss C, Albrecht J, Kuhn H, Leonhardt S and Kronmüller H 2002 Magneto-optical studies of current distributions in high-Tc superconductors *Rep. Prog. Phys.* **65** 651–788
[4] Wells F S, Pan A V, Golovchanskiy I A, Fedoseev S A and Rozenfeld A 2017 Observation of transient overcritical currents in YBCO thin films using high-speed magneto-optical imaging and dynamic current mapping *Sci. Rep.* **7** 40235
[5] Johansen T, Baziljevich M, Bratsberg H, Galperin Y and Lindelof P 1996 Direct observation of the current distribution in thin superconducting strips using magneto-optic imaging *Phys. Rev.* B **54** 16264–9
[6] Albrecht J, Brück S, Stahl C and Ruoß S 2016 Quantitative magneto-optical analysis of the role of finite temperatures on the critical state in YBCO thin films *Supercond. Sci. Technol.* **29** 114002
[7] Palau A *et al* 2016 Encoding magnetic states in monopole-like configurations using superconducting dots *Adv. Sci.* **3** 1600207
[8] Simmendinger J, Ruoss S, Stahl C, Weigand M, Gräfe J, Schütz G and Albrecht J 2018 Transmission x-ray microscopy at low temperatures: Irregular supercurrent flow at small length scales *Phys. Rev.* B **97** 134515
[9] Buzdin A I and Ryazanov V V 2006 Proximity effect in superconductor-ferromagnet heterostructures *C. R. Phys.* **7** 107–15
[10] Paull O H C, Pan A V, Causer G L, Fedoseev S A, Jones A, Liu X, Rosenfeld A and Klose F 2018 Field dependence of the ferromagnetic/superconducting proximity effect in a YBCO/STO/LCMO multilayer *Nanoscale* **10** 18995–9003
[11] Satapathy D K *et al* 2012 Magnetic proximity effect in $YBa_2Cu_3O_7/La_{2/3}Ca1/3MnO_3$ and $YBa_2Cu_3O_7/LaMnO_{3+\delta}$ superlattices *Phys. Rev. Lett.* **108** 197201
[12] Frano A *et al* 2016 Long-range charge-density-wave proximity effect at cuprate/manganate interfaces *Nat. Mater.* **15** 831–4
[13] Kalcheim Y, Millo O, Di Bernardo A, Pal A and Robinson J W A 2015 Inverse proximity effect at superconductor-ferromagnet interfaces: evidence for induced triplet pairing in the superconductor *Phys. Rev.* B **92** 060504
[14] Sillanpää M A, Heikkilä T T, Lindell R K and Hakonen P J 2001 Inverse proximity effect in superconductors near ferromagnetic material *Europhys. Lett.* **56** 590–5
[15] Ouassou J A, Di Bernardo A, Robinson J W A and Linder J 2016 Electric control of superconducting transition through a spin–orbit coupled interface *Sci. Rep.* **6** 29312
[16] Banerjee N, Ouassou J A, Zhu Y, Stelmashenko N A, Linder J and Blamire M G 2018 Controlling the superconducting transition by spin–orbit coupling *Phys. Rev.* B **97** 184521
[17] Brisbois J *et al* 2016 Imprinting superconducting vortex footsteps in a magnetic layer *Sci. Rep.* **6** 27159
[18] Aladyshkin A Y, Silhanek A V, Gillijns W and Moshchalkov V V 2009 Nucleation of superconductivity and vortex matter in superconductor-ferromagnet hybrids *Supercond. Sci. Technol.* **22** 053001
[19] Chien T Y, Kourkoutis L F, Chakhalian J, Gray B, Kareev M, Guisinger N P, Muller D A and Freeland J W 2013 Visualizing short-range charge transfer at the interfaces between ferromagnetic and superconducting oxides *Nat. Commun.* **4** 2336
[20] Albrecht J, Soltan S and Habermeier H U 2005 Magnetic pinning of flux lines in heterostructures of cuprates and manganites *Phys. Rev.* B **72** 092502
[21] Stahl C, Walker P, Treiber S, Christiani G, Schütz G and Albrecht J 2014 Using magnetic coupling in bilayers of superconducting YBCO and soft-magnetic CoFeB to map supercurrent flow *Europhys. Lett.* **106** 27002
[22] Stahl C, Ruoß S, Weigand M, Bechtel M, Schütz G and Albrecht J 2015 Low temperature x-ray imaging of magnetic flux patterns in high temperature superconductors *J. Appl. Phys.* **117** 17D109
[23] Stahl C, Gräfe J, Ruoß S, Zahn P, Bayer J, Simmendinger J, Schütz G and Albrecht J 2017 Advanced magneto-optical Kerr effect measurements of superconductors at low temperatures *AIP Adv.* **7** 105019
[24] Sen K *et al* 2016 x-ray absorption study of the ferromagnetic Cu moment at the $YBa_2Cu_3O_7/La_{2/3}Ca1/_3MnO_3$ interface and variation of its exchange interaction with the Mn moment *Phys. Rev.* B **93** 205131
[25] Blatter G, Feigel'Man M V, Geshkenbein V B, Larkin A I and Vinokur V M 1994 Vortices in high-temperature superconductors *Rev. Mod. Phys.* **66** 1125–388
[26] Theuss H and Kronmüller H 1991 The influence of a point defect structure on the magnetic properties of $YBa_2Cu_3O_{7-\delta}$ polycrystals *Physica* C **177** 253–61
[27] Yan H, Abdelhadi M M, Jung J A, Willemsen B A and Kihlstrom K E 2005 Exponential dependence of the vortex pinning potential on current density in high-Tc superconductors *Phys. Rev.* B **72** 064522
[28] Jooss C, Warthmann R, Kronmüller H, Haage T, Habermeier H U and Zegenhagen J 1999 Vortex pinning due to strong quasiparticle scattering at antiphase boundaries in $YBa_2Cu_3O_{7-\delta}$ *Phys. Rev. Lett.* **82** 632–5
[29] Opherden L *et al* 2016 Large pinning forces and matching effects in $YBa_2Cu_3O_{7-\delta}$ thin films with Ba2Y(Nb/Ta)O6 nano-precipitates *Sci. Rep.* **6** 21188
[30] Crisan A, Dang V S, Mikheenko P, Ionescu A M, Ivan I and Miu L 2017 Synergetic pinning centres in $BaZrO_3$-doped $YBa_2Cu_3O_{7-x}$ films induced by $SrTiO_3$ nano-layers *Supercond. Sci. Technol.* **30** 045012
[31] Mark A G, Gibbs J G, Lee T C and Fischer P 2013 Hybrid nanocolloids with programmed three-dimensional shape and material composition *Nat. Mater.* **12** 802–7
[32] Bean C P 1962 Magnetization of hard superconductors *Phys. Rev. Lett.* **8** 250–3
[33] Gyorgy E M, Van Dover R B, Jackson K A, Schneemeyer L F and Waszczak J V 1989 Anisotropic critical currents in $Ba_2YCu_3O_7$analyzed using an extended Bean model *Appl. Phys. Lett.* **55** 283–5
[34] Albrecht J, Djupmyr M, Soltan S, Habermeier H U, Connolly M R and Bending S J 2007 Inhomogeneous vortex distribution and magnetic coupling in oxide superconductor-ferromagnet hybrids *New J. Phys.* **9** 379

[35] Laviano F, Gozzelino L, Gerbaldo R, Ghigo G, Mezzetti E, Przyslupski P, Tsarou A and Wisniewski A 2007 Interaction between vortices and ferromagnetic microstructures in twinned cuprate/manganite bilayers *Phys. Rev.* B **76** 214501

[36] Gutiérrez J *et al* 2007 Strong isotropic flux pinning in solution-derived $YBa_2Cu_3O_{7-x}$ nanocomposite superconductor films *Nat. Mater.* **6** 367–73

[37] Pan V, Cherpak Y, Komashko V, Pozigun S, Tretiatchenko C, Semenov A, Pashitskii E and Pan A V 2006 Supercurrent transport in $YBa_2Cu_3O_{7-\delta}$ epitaxial thin films in a dc magnetic field *Phys. Rev.* B **73** 054508

[38] Albrecht J, Djupmyr M and Brück S 2007 Universal temperature scaling of flux line pinning in high-temperature superconducting thin films *J. Phys.: Condens. Matter* **19** 216211

[39] Treiber S, Stahl C, Schütz G, Soltan S and Albrecht J 2014 Stabilization of the dissipation-free current transport in inhomogeneous MgB_2 thin films *Physica* C **506** 1–5

[40] Djupmyr M, Cristiani G, Habermeier H U and Albrecht J 2005 Anisotropic temperature-dependent current densities in vicinal $YBa_2Cu_3O_{7-\delta}$ *Phys. Rev.* B **72** 220507

[41] Djupmyr M, Soltan S, Habermeier H U and Albrecht J 2009 Temperature-dependent critical currents in superconducting $YBa_2Cu_3O_{7-\delta}$ and ferromagnetic $La2/3Ca1/3MnO_3$ hybrid structures *Phys. Rev.* B **80** 184507

[42] Yeshurun Y, Malozemoff A P and Shaulov A 1996 Magnetic relaxation in high-temperature superconductors *Rev. Mod. Phys.* **68** 911–49

[43] Feigelman M V, Geshkenbein V B, Larkin A I and Vinokur V M 1989 Theory of collective flux creep *Phys. Rev. Lett.* **63** 2303–6

[44] Abulafia Y *et al* 1996 Plastic vortex creep in $YBa_2Cu_3O_{7-x}$ crystals *Phys. Rev. Lett.* **77** 1596–9

[45] Kuncser V and Miu L 2014 *Size Effects in Nanostructures* (*Springer Series in Materials Science*) (Berlin: Springer) ch 9 pp 293–317